arXiv:1411.3558v1 [astro-ph.GA] 13 Nov 2014

Classical Cepheids in the Galactic outer ring $R_1 R_2'$

A. M. Mel'nik[1⋆], **P. Rautiainen**[2], **L. N. Berdnikov**[1,3], **A. K. Dambis**[1] **& A. S. Rastorguev**[1]

[1] Sternberg Astronomical Institute, Lomonosov Moscow State University, 13 Universitetskij Prosp., Moscow 119991, Russia
[2] Department of Physics/Astronomy Division, University of Oulu, P.O. Box 3000, FIN-90014 Oulun yliopisto, Finland
[3] Astronomy and Astrophysics Research division, Entoto Observatory and Research Center, P.O.Box 8412, Addis Ababa, Ethiopia

Received 2014, accepted 2014
Published online 2014

Key words Galaxy: structure – Galaxy: kinematics and dynamics – (stars: variables:) Cepheids – galaxies: spiral

The kinematics and distribution of classical Cepheids within ~ 3 kpc from the Sun suggest the existence of the outer ring $R_1 R_2'$ in the Galaxy. The optimum value of the solar position angle with respect to the major axis of the bar, θ_b, providing the best agreement between the distribution of Cepheids and model particles is $\theta_b = 37 \pm 13^\circ$. The kinematical features obtained for Cepheids with negative Galactocentric radial velocity V_R are consistent with the solar location near the descending segment of the outer ring R_2. The sharp rise of extinction toward of the Galactic center can be explained by the presence of the outer ring R_1 near the Sun.

Copyright line will be provided by the publisher

1 Introduction

Classical Cepheids – F–K-type supergiants with ages from 20 to 200 Myr (Efremov 2003, Bono et al. 2005) – are good tracers of the Galactic spiral structure and regions of high gas density. Due to the period-luminosity relation the distances to classical Cepheids can be determined with an accuracy of $\sim 10\%$ (Berdnikov, Dambis & Vozyakova 2000; Sandage & Tammann 2006).

Most of the recent studies of the spiral structure of the Galaxy (see e.g. the review by Vallée (2013) and references therein) have typically suggested a 2- or 4-armed spiral pattern with a pitch angle of nearly $i = 6^\circ$ or 12°, respectively. In our previous studies (Mel'nik & Rautiainen 2009; Rautiainen & Mel'nik 2010) we proposed an alternative to these purely spiral models – a two-component outer ring $R_1 R_2'$.

The main advantage of the 4-armed spiral model is that it can explain the distribution of HII regions in the Galactic disk (Georgelin & Georgelin 1976; Russeil 2003; and other papers) and the existence of so-called tangential directions related to the maxima in the thermal radio continuum, HI and CO emission which are associated with the tangents to the spiral arms (Englmaier & Gerhard 1999; Vallée 2008).

The main shortcoming of this approach is the absence of a dynamical mechanism to maintain the global spiral pattern for a long time period (more than a few disk rotations) (Toomre 1977; Athanassoula 1984). Generally, the bar could support the spiral pattern, but in this case the spiral pattern must rotate with the angular velocity of the bar ($\Omega_s = \Omega_b$) (Englmaier & Gerhard 1999). The estimates of the corotation radius (CR) of the Galactic bar do not exceed 5 kpc, which gives the lower limit for its angular velocity $\Omega_b > 40$ km s^{-1} kpc^{-1} (Weiner & Sellwood 1999). However, this model cannot explain the kinematics of the Perseus region: the direction of the velocities of young stars in the Perseus region, if interpreted in terms of the density-wave concept (Lin, Yuan & Shu 1969), indicates that a fragment of a Perseus arm must be located inside the corotation circle (CR) (Burton & Bania 1974; Mel'nik, Dambis & Rastorguev 2001; Mel'nik 2003; Sitnik 2003) implying an upper limit $\Omega_s < 25$ km s^{-1} kpc^{-1} for its pattern speed, which is inconsistent with the one mentioned above. Attempts have been undertaken to overcome this contradiction by introducing an analytical spiral potential rotating slower than the bar (Bissantz, Englmaier & Gerhard 2003). Note that numerical simulations show that galactic stellar disks can develop modes that rotate slower than the bar (Sellwood & Sparke 1988; Masset & Tagger 1997; Rautiainen & Salo 1999, 2000). However, it is questionable whether the amplitude of slow modes can be large enough to determine the kinematics at twice the radius of the CR of the Galactic bar.

Another concept of the Galactic spiral structure is that the disk rather than global modes forms transient spiral arms. Sellwood (2000, 2010) advances the idea that fresh and decaying instabilities are connected through resonances, which is based on some specific features in the angular momentum distribution of old stars in the solar vicinity. Baba et al. (2009) build a model of the Galaxy with transient spiral arms, which can explain the large peculiar velocities, 20–30 km s^{-1}, of maser sources in the Galactic disk. Transient spiral arms must heat the galactic disk in few disk rotation periods (Sellwood & Carlberg 1984). We can

⋆ Corresponding author. e-mail: anna@sai.msu.ru

Copyright line will be provided by the publisher

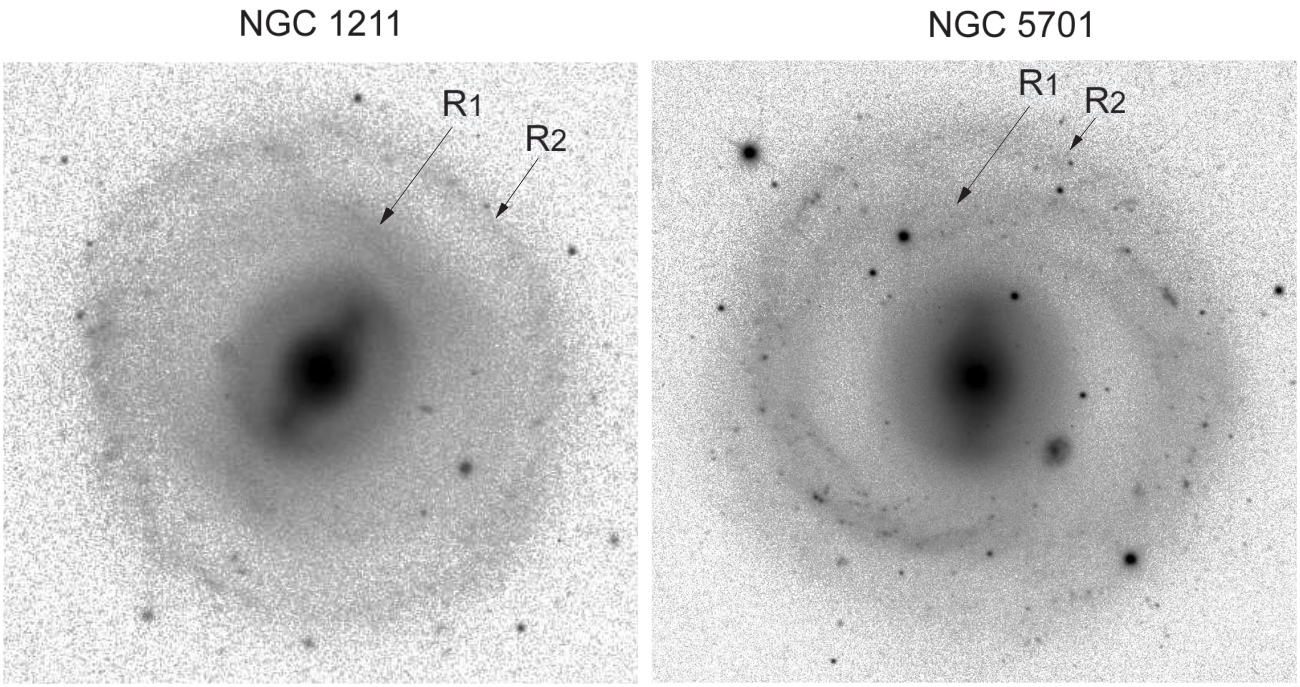

Fig. 1 Galaxies NGC 1211 and NGC 5701 with outer ring morphology R_1R_2. The g-band images were taken from NASA-Sloan Atlas (http://www.nsatlas.org/) created by Michael Blanton et al. (see also Blanton et al. 2011). The images were obtained in green filter centered at 477 nm during the program of the Sloan Digital Sky Survey (York et al., 2000). The images demonstrate two outer rings oriented perpendicular to each other. Of the two rings, R_1 is located a bit closer to the galactic center than the R_2.

suggest that young massive stars born in such arms should also acquire large peculiar velocities. However, young stellar objects (classical Cepheids, young open clusters, OB-associations) in the wide solar neighborhood move in nearly circular orbits with average velocity deviations of 7–13 km s^{-1} from the rotation curve (Zabolotskikh, Rastorguev & Dambis 2002; Mel'nik & Dambis 2009; Bobylev & Baikova 2012; and other papers).

Models of the Galaxy with the outer ring R_1R_2' can reproduce well the radial and azimuthal components of the residual velocities (after substracting the velocity due to the rotation curve and the solar motion to the apex) of OB-associations in the Sagittarius and Perseus stellar-gas complexes identified by Efremov & Sitnik (1988). The radial velocities of most OB-associations in the Perseus region are directed toward the Galactic center and this indicates the presence of the ring R_2 in the Galaxy, while the radial velocities in the Sagittarius region are directed away from the Galactic center suggesting the existence of the ring R_1. The nearly zero azimuthal component of the residual velocity of most OB-associations in the Sagittarius region precisely constrains the solar position angle with respect to the bar major axis, $\theta_b = 45 \pm 5^\circ$. We considered models with analytical bars and N-body simulations (Mel'nik & Rautiainen 2009; Rautiainen & Mel'nik 2010).

Models of a two-component outer ring are consistent with the (l, V_{LSR}) diagram by Dame, Hartmann & Thaddeus (2001). These models can explain the position of the Carina arm with respect to the Sun and with respect to the bar. They can also explain the existence of some of the tangential directions corresponding to the emission maxima near the terminal velocity curves which, in this case, can be associated with the tangents to the outer and inner rings. Our model diagrams (l, V_{LSR}) reproduce the maxima in the direction of the Carina, Crux (Centaurus), Norma, and Sagittarius arms. Additionally, N-body model yields maxima in the directions of the Scutum and 3-kpc arms (Mel'nik & Rautiainen 2011, 2013).

The elliptic outer rings can be divided into the ascending and descending segments: in the ascending segments Galactocentric distance R decreases with increasing azimuthal angle θ, which itself increases in the direction of Galactic rotation, whereas the dependence is reversed in the descending segments. Ascending and descending segments of the rings can be regarded as fragments of trailing and leading spiral arms, respectively. Note that if considered as fragments of the spiral arms, the ascending segments of the outer ring R_2 have the pitch angle of $\sim 6^\circ$ (Mel'nik & Rautiainen 2011).

Two main classes of outer rings and pseudorings (incomplete rings made up of two tightly wound spiral arms) have been identified: rings R_1 (pseudorings R_1') elongated perpendicular to the bar and rings R_2 (pseudorings R_2') elongated parallel to the bar. In addition, there is a combined morphological type R_1R_2' which exhibits elements of both classes (Buta 1995; Buta & Combes 1996; Buta & Crocker 1991; Comeron et al. 2013). Modelling shows that outer rings are usually located near the OLR of the bar

Copyright line will be provided by the publisher

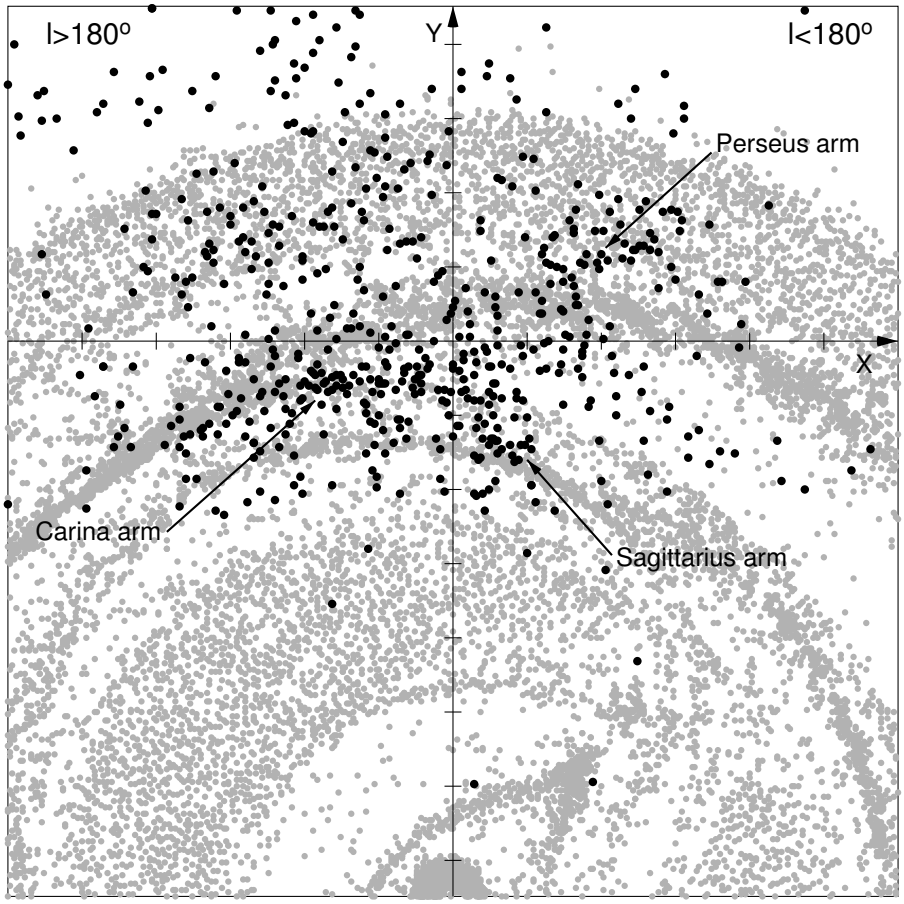

Fig. 2 Distribution of classical Cepheids (black circles) and model particles (gray circles) in the Galactic plane. For model particles the solar position angle is chosen to be $\theta_b = 45^\circ$. The arrows indicate the positions of the Sagittarius, Carina, and Perseus arm-fragments. The X-axis points in the direction of Galactic rotation and the Y-axis is directed away from the Galactic center. One tick interval along the X- and Y-axis corresponds to 1 kpc. The Sun is at the origin. We can see a fork-like structure in the distribution of Cepheids: on the left ($l > 180^\circ$) Cepheids strongly concentrate to the only one arm (the Carina arm), while on the right ($l < 180^\circ$) there are two arm-fragments located near the Perseus and Sagittarius regions.

(Schwarz 1981; Byrd et al. 1994; Rautiainen & Salo 1999, 2000; and other papers). However, the ring R_1 can be located further inwards, closer to the outer 4/1-resonance in some cases (Treuthardt et al. 2008).

Buta and Combes (1996) have shown that for the galaxies in the lower red-shift range the frequency of the outer rings is 10% of all types of spiral galaxies. However, it increases to 20% for the early-type sample. Note, however, that Comeron et al. (2014) obtained a larger frequency from an analysis of the data from mid-infrared survey (Spitzer Survey of Stellar Structure in Galaxies, Sheth at al. 2010): 16% for all spiral galaxies located inside 20 Mpc and over 40% for disk galaxies of early morphological types (galaxies with large bulges). They have also found that the frequency of outer rings increases from $15 \pm 2\%$ to $32 \pm 7\%$ when going through the family sequence from SA to SAB, and decreases again to $20 \pm 2\%$ for SB galaxies. The catalog of Southern Ringed Galaxies by Buta (1995) gives the following statistics of the main ring classes: 18% (R_1), 37% (R'_1), under 1% (R_2), 35% (R'_2), and 9% ($R_1R'_2$). Comeron et al. (2014) generally confirm these results: $35 \pm 18\%$ of outer rings in barred galaxies are parallel to the bar and $65 \pm 39\%$ are oriented perpendicular to it. The small fraction of galaxies with $R_1R'_2$ rings may be due to the selection effects – the rings R_2 are often weaker than rings R_1, moreover rings R_2 are often appear more conspicuous when observed in the B-band. The completeness of the catalogs regarding the R_2 features is difficult to estimate. Generally, the frequency of galaxies with outer rings $R_1R'_2$ among barred galaxies may be as high as few per cent. Note that the catalog by Buta (1995) includes several tens of galaxies with rings $R_1R'_2$.

Figure 1 shows two galaxies with R_1R_2 outer ring morphology. The g-band images of galaxies NGC 1211 and NGC 5701 were taken from NASA-Sloan Atlas (http://www.nsatlas.org/) created by Michael Blanton et al. (see also Blanton et al. 2011). The images were obtained in green filter centered at 477 nm during the program of the Sloan Digital Sky Survey (York et al., 2000). The images demonstrate two outer rings oriented perpendicu-

Copyright line will be provided by the publisher

lar to each other. Of the two rings, R_1 is located a bit closer to the galactic center than the R_2. Other examples of galaxies with the R_1R_2' morphology that can also be viewed as possible prototypes of the Galaxy are ESO 245-1, NGC 1079, NGC 3081, NGC 5101, NGC 6782, and NGC 7098. Their images can be found in de Vaucouleurs Atlas of Galaxies by Buta, Corwin, Odewahn (2007) at http://bama.ua.edu/∼rbuta/devatlas/

Schwarz (1981) associates two main types of outer rings with two main families of periodic orbits existing near the OLR of the bar (Contopoulos & Papayannopoulos 1980). The main periodic orbits $x_1(1)$ and $x_1(2)$ (in terms of the nomenclature of Contopoulos & Grosbol 1989) are followed by numerous chaotic orbits, and this guidance enables elliptical rings to hold a lot of gas in their vicinity. The rings R_1 are supported by $x_1(2)$-orbits lying inside the OLR and elongated perpendicular to the bar while the rings R_2 are supported by $x_1(1)$-orbits located slightly outside the OLR and elongated along the bar. However, the role of chaotic and periodic orbits appears to be different in the center region and on the galactic periphery: chaos is dominant outside the CR, while most orbits in the bar are ordered (Contopoulos & Patsis 2006; Voglis, Harsoula & Contopoulos 2007; Harsoula & Kalapotharakos 2009). Probably, it is not only periodic orbits associated with the OLR that are responsible for the formation of the outer rings/pseudorings. A concept has been proposed that the formation of outer rings as well as that of spiral arms is determined by manifolds associated with the Lagrangian points L1 and L2 (Romero-Gómez et al. 2007; Athanassoula et al. 2010).

The existence of the bar in the Galaxy is confirmed by numerous infra-red observations (Blitz & Spergel 1991; Benjamin et al. 2005; Cabrera-Lavers et al. 2007; Churchwell et al. 2009, González-Fernández et al. 2012) and by gas kinematics in the central region (Binney et al. 1991; Englmaier & Gerhard 1999; Weiner & Sellwood 1999). The general consensus is that the major axis of the bar is oriented in the direction $\theta_b = 15$–45° in such a way that the end of the bar closest to the Sun lies in quadrant I. The semi-major axis of the Galactic bar is supposed to lie in the range $a = 3.5$–5.0 kpc. Assuming that its end is located close to its corotation radius, i.e. we are dealing with a so-called fast bar (Debattista & Sellwood 2000), and that the rotation curve is flat, we can estimate the bar angular speed Ω_b which appears to be constrained to the interval $\Omega_b = 40$–65 km s^{-1} kpc^{-1}. This means that the OLR of the bar is located in the solar vicinity: $|R_{OLR} - R_0| < 1.5$ kpc. Studies of the kinematics of old disk stars in the nearest solar neighborhood, $r < 250$ pc, reveal the bimodal structure of the distribution of (u, v) velocities which is also interpreted as a result of the solar location near the OLR of the bar (Kalnajs 1991; Dehnen 2000; Fux 2001; and other papers).

In this paper we show that the morphological and kinematical features of the Cepheid sample considered are consistent with the presence of a ring R_1R_2' in the Galaxy. Section 2 describes the models and catalogues used; Section 3 considers the special features in the distribution of Cepheids; Section 4 studies the kinematics of Cepheids, and Section 5 presents the main results and their discussion.

2 Models, catalogues, and calibrations

We used the catalogue of classical Cepheids by Berdnikov et al. (2000) which is continuously improved and updated by incorporating new observations (Berdnikov et al. 2009a, 2009b, 2011, 2014). The last version of the catalogue includes the data for 674 Cepheids (Berdnikov, Dambis & Vozyakova 2014, in preparation). The procedure of deriving distances is based on the K-band period-luminosity relation of Berdnikov, Vozyakova & Dambis (1996b) and interstellar-extinction law derived in Berdnikov, Vozyakova & Dambis (1996a). The interstellar-extinction values are estimated using the $B - V$ period-color relation of Dean, Warren, and Cousins (1978). Note the natural spread of the period-color relation does not introduce any substantial errors in the inferred distance values because the K-band extinction is very small, A_K = 0.274E_{B-V}. Our procedure in this case is essentially equivalent to using the Vm_λ Wesenheit function with the deviations from the mean period-luminosity and period-color relations virtually cancelling each other (Berdnikov et al. 1996a). Note the variations in the distance scale up to 10% do not affect our conclusions.

We use the simulation code developed by H. Salo (Salo 1991; Salo & Laurikainen 2000) to construct two different types of models (models with analytical bars and N-body simulations) which reproduce the kinematics of OB-associations in the Perseus and Sagittarius regions. Among many models with outer rings, we chose model 3 from the series of models with analytical bars (Mel'nik & Rautiainen 2009) for comparison with observations. This model has nearly flat rotation curve. The bar semi-axes are equal to $a = 4.0$ kpc and $b = 1.3$ kpc. The positions and velocities of 5×10^4 model particles (gas+OB) are considered at time $T = 15$ (∼1 Gyr). We scaled and turned this model with respect to the Sun to achieve the best agreement between the velocities of model particles and those of OB-associations in five stellar-gas complexes (Efremov & Sitnik 1988).

We adopt a solar Galactocentric distance of $R_0 = 7.5$ kpc (Rastorguev et al. 1994; Dambis, Mel'nik & Rastorguev 1995; Glushkova et al. 1998; Nikiforov 2004; Feast et al. 2008; Groenewegen, Udalski & Bono 2008; Reid et al. 2009b; Dambis et al. 2013). As model 3 was adjusted for $R_0 = 7.1$ kpc, we rescaled all distances for model particles by a factor of $k = 7.5/7.1$. Note that the analysis of morphology and kinematics of stars located within 3 kpc from the Sun is practically independent of the choice of R_0 in the range 7–9 kpc.

Table 1, which is available in the online version of the paper, gives the positions, line-of-sight velocities and proper motions of classical Cepheids. It ia also available at:

http://lnfm1.sai.msu.ru/∼anna/tables/tables_2014.zip

Copyright line will be provided by the publisher

It includes 674 classical Cepheids from the new release of the catalog of classical Cepheids by Berdnikov et al. (2014, in preparation). For every classical Cepheid we give its designation in the General Catalog of Variable Stars (GCVS) (Samus at al. 2007) or in the All Sky Automated Survey (ASAS) (Pojmanski 2002), its type (see GCVS description), fundamental period P_F, intensity-mean V-band magnitude, J2000 equatorial coordinates α and δ, galactic coordinates l and b, and heliocentric distance r. Table 1 also gives the Cepheid line-of-sight velocities V_r (the so-called γ-velocities, see Metzger, Caldwell & Schechter 1992), their uncertainties ε_{Vr} and the references (1–6) to the sources from which they are taken. The proper motions of Cepheids were adopted from the new reduction of Hipparcos data (ESA 1997) by van Leeuwen (2007). Table 1 presents proper motions μ_α and μ_δ, their uncertainties $\varepsilon_{\mu\alpha}$ and $\varepsilon_{\mu\delta}$ and the corresponding Hipparcos catalog number n_{Hip}.

Table 2 lists the catalogs of line-of-sight velocities used in our study. For each catalog it gives the corresponding reference number used in Table 1, the authors of the catalog, the full reference to the paper/catalog, and the number of velocities taken from each source. Some sources include a series of papers by one group of researches and/or data available only online.

3 Morphological evidence

3.1 Distribution in the Galactic plane

The distribution of Cepheids in the Galactic plane can reveal regions of high gas density which can be associated with spiral arms or Galactic rings. Figure 2 shows the distributions of classical Cepheids and model particles. We can notice two specific features here. First, the distribution of Cepheids is reminiscent of "a tuning fork": at longitudes $l > 180^\circ$ there is only one spiral arm (the Carina arm) toward which Cepheids concentrate strongly while at longitudes $l < 180^\circ$ there are two regions with high surface density located near the Perseus and Sagittarius regions. Second, the concentration of Cepheids drops sharply in the direction to the Galactic center while it decreases more gradually in other directions. These features will be studied further.

We also provide Figure 3 to emphasize the fork-like structure in the distribution of Cepheids. Positions of Cepheids are represented in coordinates (θ, ΔR), where θ is the Galactocentric angle and $\Delta R = R - R_0$ is the difference between the Galactocentric distances of a Cepheid and the Sun. Cepheids can be seen to concentrate to the Carina arm at the negative angles θ and to the Perseus and Sagittarius regions at the positive θ.

The position of two outer rings in the distribution of model particles can be approximated by two ellipses oriented perpendicular to each other. The outer ring R_1 can be represented by the ellipse with the semi-axes $a_1 = 6.3$ and $b_1 = 5.8$ kpc, while the outer ring R_2 fits well the ellipse with $a_2 = 8.5$ and $b_2 = 7.6$ kpc. These values correspond to the solar Galactocentric distance $R_0 = 7.5$ kpc. The ring R_1 is stretched perpendicular to the bar and the ring R_2 is aligned with the bar, hence the position of the Sun and that of the sample of Cepheids with respect to the rings is determined by the Galactocentric angle θ_b of the Sun with respect to the major axis of the bar. We now assume that Cepheids concentrate to the outer rings to find the optimum angle θ_b providing the best agreement between the position of the rings and the distribution of Cepheids.

Figure 4 shows three χ^2 functions – the sum of normalized squared deviations of Cepheids from the outer rings (Press et al. 1987) – calculated for different values of the angle θ_b. For each star we determined the minimum distances to the two ellipses and then took the smallest of the two values. However, the χ^2 function appears to be very sensitive to the completeness of the sample. This problem will be studied further. Here we show the results obtained for three distance-limited Cepheid samples including stars located within $r_{max} = 2.5$, 3.0, and 3.5 kpc from the Sun. Table 3 lists the parameters of different samples: the number N of Cepheids, the minimal value χ^2_{min}, the standard deviation σ_0 of a Cepheid from the model distribution, and the angle θ_b corresponding to χ^2_{min}. In this section we consider the parameters derived without any segregation over periods, deferring the discussion of the values obtained for short- and long-period Cepheids separately to section 3.2. The first three rows of Table 3 indicate that the χ^2 functions reach their minima at $\theta_b = 50^\circ$, 37°, and 25°, respectively. The random errors of these estimates are of about $\pm 5^\circ$. Note that the different values of χ^2_{min} represented in Table 3 are derived for different samples and cannot be compared with each other. This also holds true for the values of σ_0.

The position angle estimates $\theta_b = 50 \pm 5^\circ$ and $37 \pm 5^\circ$ derived for the samples within $r_{max} = 2.5$ and 3.0 kpc, respectively, agree well with the estimate $\theta_b = 45 \pm 5^\circ$ obtained from the kinematics of OB-associations (Mel'nik & Rautiainen 2009; Rautiainen & Mel'nik 2010). It must be "the fork-shaped" distribution of Cepheids that determines the angle θ_b being close to 45°. At longitudes $l > 180^\circ$ two outer rings fuse together to form one spiral fragment – the Carina arm, whereas at longitudes $l < 180^\circ$ two outer rings are prominent, generating the fragments of the Sagittarius and Perseus arms.

We can see that the estimates of θ_b decrease with increasing r_{max} (Table 3). This shift can be attributed to numerous stars scattered in the direction of the anti-center at distances $r > 2$ kpc (Figures 2,3). Their inclusion into the sample makes the outer ring R_2 to be aligned with the line connecting the Sun and the Galactic center. As the ring R_2 is aligned with the bar, the increase of r_{max} must be accompanied by the decrease in θ_b.

On the whole, the optimum position angle θ_b providing the best agreement between the distribution of Cepheids inside 3 ± 0.5 kpc and the model of the outer ring $R_1 R_2'$ can

Copyright line will be provided by the publisher

Table 2 Sources of Cepheid line-of-sight velocities

Ref.	Authors	year	journal	number
	Metzger et al.	1991	ApJS, 76, 803	
	Metzger, Caldwell & Schechter	1992	AJ, 103, 529	
1	Metzger, Caldwell & Schechter	1998	AJ, 115, 635	191
	Gorynya et al.	1992	Sov. Astron. Lett., 18, 316	
	Gorynya et al.	1998	Astron. Lett., 24, 815	
	Gorynya et al.	2002	VizieR On-line Data Catalog: III/229	
2	Gorynya & Rastorguev	2014	in preparation	86
	Pont, Mayor & Burki	1994	A&A, 285, 415	
3	Pont et al.	1997	A&A, 318, 416	36
4	Barbier-Brossat, Petit & Figon	1994	A&AS, 108, 603	7
5	Malaroda, Levato & Gallianiet	2006	VizieR On-line Data Catalog: III/249	2
6	Fernie et al.	1995	IBVS, 4148, 1	6

Table 3 Parameters of different samples of Cepheids

Period	r_{max}	N	χ^2_{min}	σ_0	θ_b
	2.5 kpc	314	312.15	0.72 kpc	$50 \pm 5^\circ$
All	3.0 kpc	372	415.17	0.81 kpc	$37 \pm 5^\circ$
periods	3.5 kpc	413	540.57	0.90 kpc	$25 \pm 5^\circ$
$P < 8$ d	2.5 kpc	242	235.88	0.71 kpc	$53 \pm 5^\circ$
$P < 8$ d	3.0 kpc	281	358.64	0.81 kpc	$40 \pm 5^\circ$
$P < 8$ d	3.5 kpc	326	521.97	0.91 kpc	$28 \pm 5^\circ$
$P > 8$ d	2.5 kpc	72	75.33	0.74 kpc	$43 \pm 10^\circ$
$P > 8$ d	3.0 kpc	91	106.80	0.78 kpc	$30 \pm 10^\circ$
$P > 8$ d	3.5 kpc	105	153.16	0.87 kpc	$23 \pm 10^\circ$

be derived by averaging the θ_b estimates listed in the first three rows of Table 3, yielding $\theta_b = 37^\circ$. The average scatter of these estimates is $\pm 12^\circ$. Assuming that two errors in the determination of θ_b, ± 12 and ± 5, are independent, we can estimate the combined error as $\varepsilon^2 = \varepsilon_1^2 + \varepsilon_2^2$, or $\sim 13^\circ$.

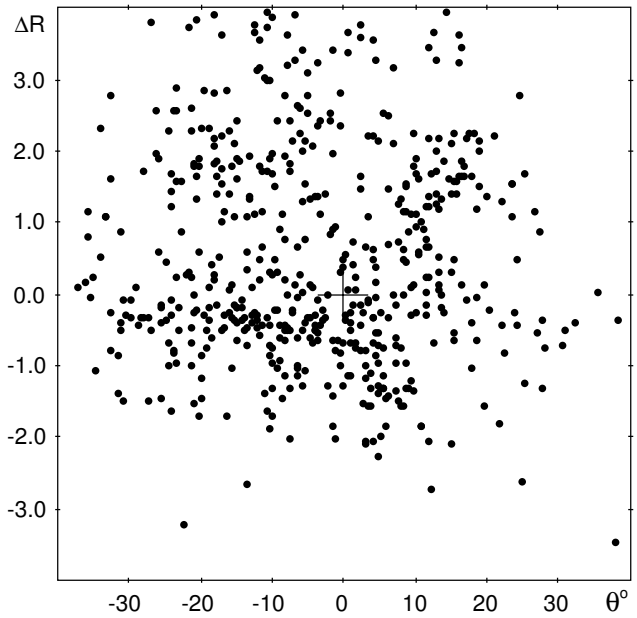

Fig. 3 Fork-like structure in the distribution of classical Cepheids (black circles). Positions of Cepheids are represented in coordinates (θ, ΔR), where θ is the Galactocentric angle and $\Delta R = R - R_0$ is the difference between the Galactocentric distances of a Cepheid and the Sun. The position of the Sun is shown by a cross. We can see the concentration of Cepheids to the Carina arm at the negative angles θ and their concentration to the Perseus and Sagittarius regions at the positive angles θ.

3.2 Distribution over periods

There is a wide-spread opinion that only classical Cepheids with long periods are suitable for study of the Galactic structure. Note that Cepheids with the periods $P < 4$ days actually require more thorough study for classification. First, some of them are oscillating in the first overtone rather than in the fundamental tone and this fact should be taken into ac-

Copyright line will be provided by the publisher

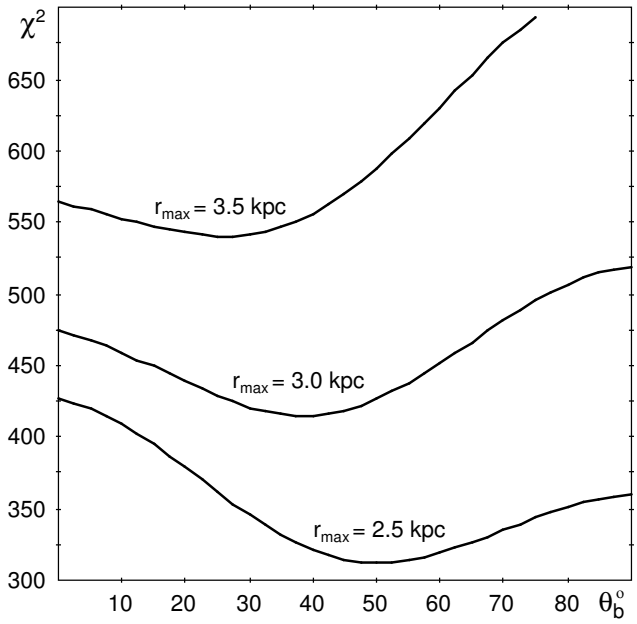

Fig. 4 The χ^2 functions calculated for different values of the solar position angle θ_b with respect to the major axis of the bar. Cepheids of all periods are included. Three distance-limited samples of Cepheids confined by $r_{max} = 2.5$, 3.0, and 3.5 kpc are considered. The χ^2 functions reach their minima at $\theta_b = 50^\circ$, 37°, and 25°, respectively.

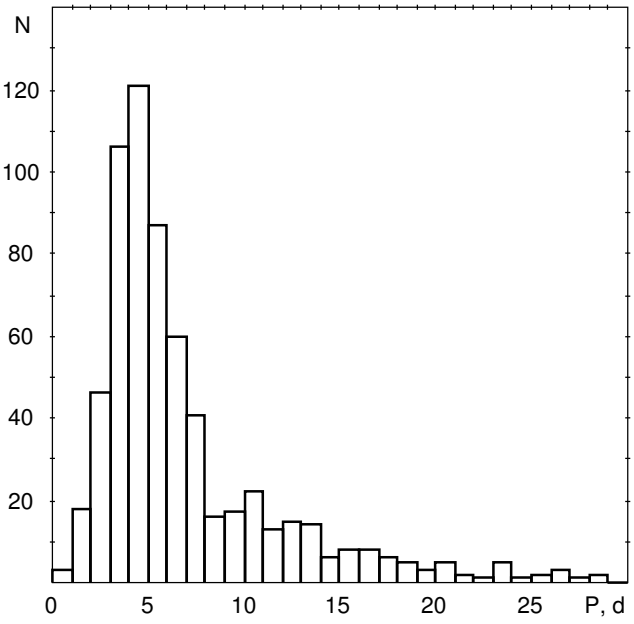

Fig. 5 The number distribution of classical Cepheids from the catalog by Berdnikov et al. (2000) over fundamental periods P.

count when computing the distances. Second, short-period classical Cepheids can be confused with W Vir type variables which are old stars of population II. However, classical Cepheids have very specific features in light curves (Hertzsprung Progression) (Hertzsprung, 1926) which distinguish them from Cepheids of other types.

The subdivision of Cepheids into long- and short-period groups is a matter of convention. Usually, they are separated by the period of 10 days. However, we believe that the value of 8 days is more appropriate. Figure 5 shows the distribution of fundamental periods of Cepheids. We can see a clear maximum in the distribution of Cepheids with periods $P < 8$ days and almost a plateau distribution for Cepheids with $P > 8$.

Figure 6 shows the distribution of classical Cepheids with short ($P < 8$ d) and long ($P > 8$ d) periods in the Galactic plane. It shows a conspicuous lack of long-period Cepheids in quadrant III. However, short- and long-period Cepheids generally show a similar behavior: they concentrate to the Carina arm in quadrant IV, to the Sagittarius region in quadrant I, and to the Perseus region in quadrant II.

We repeat our study of the χ^2 functions for short- and long-period Cepheids separately. Table 3 presents the parameters derived for Cepheids with periods $P < 8$ and $P > 8$ days in three regions: $r_{max} = 2.5$, 3.0, and 3.5 kpc. We can see that the angles θ_b corresponding to χ^2_{min} derived for the short- and long-period Cepheids in the same regions coincide within the errors. On the whole, short- and long-period Cepheids demonstrate the same tendency.

3.3 Average surface density and extinction in different directions

The average surface density and interstellar extinction of Cepheids in different directions can provide us with additional information about the distribution of gas and dust in the Galaxy. To study these characteristics, we subdivide the sample of Cepheids into four sectors: the directions to the center $|l| < 45^\circ$ and anti-center $|l-180| < 45^\circ$, those in the sense of Galactic rotation $|l-90| < 45^\circ$ and in the opposite sense $|l-270| < 45^\circ$. For each sector we calculate the number of Cepheids in annuli of width $\Delta r = 1$ kpc. The ratio of the number of Cepheids in a quarter of an annulus to its area gives us the average surface density n of Cepheids per kpc^2. This value depends on the sector and heliocentric distance r. We also calculate the average V-band extinction A_V for Cepheids in different annuli and in different sectors. We compute the A_V value for each star as $A_V = 3.26E_{B-V}$ (Berdnikov et al. 1996a), where E_{B-V} is the color excess from the catalog by Berdnikov et al. (2000). Note that the values of A_V were not used in the determination of Cepheid distances which were derived from the K-band magnitudes and extinction A_K (see also section 2).

Figure 7 (a) and (b) shows the variations of $n(r)$ and $A_V(r)$ along the heliocentric distance r calculated for the four sectors. The surface density of Cepheids n in the direction of the center ($|l| < 45^\circ$) can be seen to drop sharply with increasing r: it decreases by a factor of ~ 10 from the distance range of 0–1 kpc to that of 2–3 kpc. For comparison, this ratio amounts only 1.3–1.9 for the other three sectors. The surface density of Cepheids in the direction of the anti-center $|l - 180| < 45^\circ$ is less than in other directions within 4 kpc, for larger distances the estimates of n are

Copyright line will be provided by the publisher

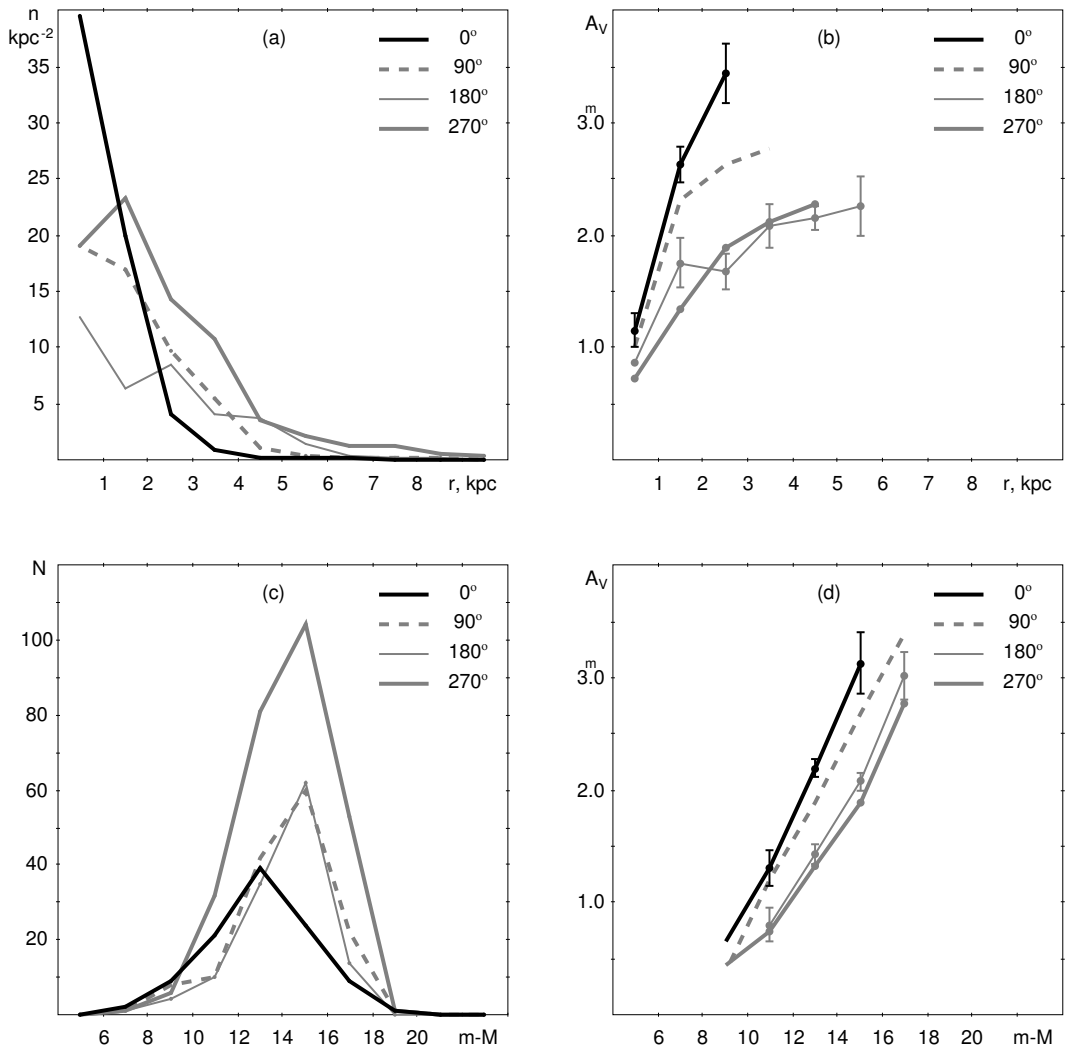

Fig. 7 (a) Variations of the average surface density n of Cepheids along the heliocentric distance r. (b) Variations of the average extinction A_V along the distance r. (c) Distribution of number of Cepheids N by the apparent distance modulus $m - M$, where N is calculated in 2^m-wide intervals of distance modulus. (d) Growth of A_V with the increasing $m - M$. Different lines show the values calculated for four sectors confined by the longitudes: $l = 0 \pm 45°$, $l = 180 \pm 45°$, $l = 90 \pm 45°$, and $l = 270 \pm 45°$. Frame (a) demonstrates the sharp drop of $n(r)$ in the direction of the Galactic center $|l| < 45°$ (black solid line). Frame (c) shows that the distribution of N in the direction of the Galactic center peaks at 13^m, whereas those for the other sectors peak at 15^m. The bars in frames (b) and (d) indicate the errors of A_V which are shown only for the direction of the Galactic center and anti-center, in other sectors they are less than 0.2^m. It is evident from frames (b) and (d) that extinction A_V in the direction of Galactic center $|l| < 45°$ is greater than in other sectors.

very uncertain. Extinction A_V can also be seen to increase sharply toward the Galactic center ($|l| < 45°$).

Additionally, we consider the variations in the number of Cepheids N and A_V along the apparent distance modulus $m - M$ (Figure 7cd), where N and the average extinction A_V are calculated in 2^m-wide distance modulus bins. The distribution of N for the sector $|l| < 45°$ peaks at 13^m, whereas those for the other sectors peak at 15^m. It means that Cepheids can generally be discovered out to $m - M = 15^m$ with the current instruments. Probably, the number of Cepheids N in the sector $|l| < 45°$ drops considerably beyond 13^m due to their lower surface density there. However, the alternative explanation is that crowding is much stronger in the direction of the Galactic center $|l| < 45°$, preventing the discovery of Cepheids. Possibly, the survey VISTA variables in the Via Lactea (Saito et al. 2012) would help solve this alternative.

The bars in Figure 7 (b) and (d) indicate the errors in extinction A_V which are shown only for the direction of the Galactic center $|l| < 45°$ and anti-center $|l-180| < 45°$. In other sectors, the errors of A_V are less than 0.2^m. We can see that extinction A_V in the direction of the Galactic center $|l| < 45°$ is greater than in other directions. Particularly, for distance moduli $m-M > 11^m$ ($r > 1.5$ kpc), the extinction A_V in the direction $|l| < 45°$ is greater than in the opposite direction $|l - 180| < 45°$ at a significance level of $P > 2\sigma$.

Copyright line will be provided by the publisher

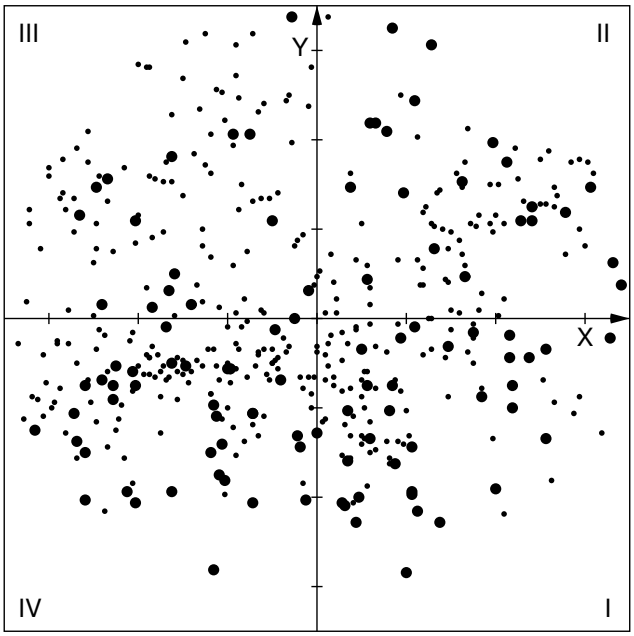

Fig. 6 The distribution of classical Cepheids with short (small circles) and long (large circles) periods in the Galactic plane within 3.5 kpc from the Sun. Periods are divided into two groups with respect of $P = 8$ days. Roman numbers indicate quadrants. We can see the conspicuous lack of long-period Cepheids in quadrant III.

Generally, these particularities can be explained in terms of the model of the Galaxy with the outer rings located near the Sun. It is probable that the line of sight directed toward the Galactic center intersects the outer ring R_1 (Figure 2) which may contain a great amount of dust. Note that N-body simulations show that the ring R_1 forms not only in the gas subsystem but also in the stellar component (Rautiainen & Salo 2000). We can expect that a high concentration of old stars in the ring R_1 can be accompanied by a great amounts of dust there.

3.4 Completeness of the sample

To estimate the radius of completeness of our sample, we need a hypothesis about the physical distribution of Cepheids. On the one hand, Cepheids should not be distributed uniformly in the Galactic disk, they must concentrate to spiral arms or to Galactic rings. On the other hand, Cepheids at larger distances are less likely to be discovered than those situated close to the Sun. Let us suppose that spiral arms or outer rings can increase the surface density of Cepheids not more than by a factor of two. That gives us a simple criterion: the sample is complete until the surface density n(r) drops not more than to half its maximum value. When applied to the four sectors this criterion suggests that our sample is complete out to 2 kpc in the direction of the Galactic center ($|l| < 45^\circ$), out to 3 kpc in two directions: that of the anti-center $|l - 180| < 45^\circ$ and in the sense of Galactic rotation $|l - 90| < 45^\circ$, and out to ~ 4 kpc in the sense opposite that of Galactic rotation $|l-270| < 45^\circ$ (Figures 7a). The latter result may be due to the great interest of observers in the Carina arm and its extension.

Another criterion of the completeness of the sample can be formulated on the basis of variations in the number of Cepheids N along the visual distance modulus $m-M$ (Figure 7b). Suppose that the sample is complete until the number of Cepheid N increases with increasing $m-M$. This establishes the limits of $m-M = 13^m$ for the sector in the direction of the Galactic center ($|l| < 45^\circ$) and $m-M = 15^m$ for the three other sectors. To transform these apparent distance moduli into distances, we must make an assumption about extinction. The variation of A_V with distance modulus (Figure 7d) shows that the average extinction at $m - M = 13^m$ in the sector ($|l| < 45^\circ$) is nearly 2.0^m and it is also close to $A_V = 2.0^m$ at $m - M = 15^m$ in three other sectors. So we can suppose that a Cepheid will be discovered if its true distance modulus is $(m - M)_0 = 11.0^m$ in the sector ($|l| < 45^\circ$) and $(m - M)_0 = 13.0^m$ in other sectors, i.e if it is located within $r = 1.6$ kpc and $r = 4.0$ kpc, respectively which is consistent with our previous estimates.

Let us consider another criterion of completeness which is based on the distribution of apparent magnitudes (Szabados 2003, for example). Figure 9 shows the distribution of apparent visual magnitudes m_v of Cepheids from the catalog by Berdnikov et al. (2000). The number of Cepheids can be seen to increase with m_v till the value 12^m. Note that the average apparent magnitudes m_v of Cepheids in the heliocentric distance intervals 2–3 and 3–4 kpc are 11 and 12^m, respectively. So again we can suppose that the catalog by Berdnikov et al. (2000) is nearly complete till ~ 3 kpc. To formulate more precisely, the incompleteness is getting obvious at $r > 3$ kpc.

4 Kinematical evidence

4.1 Rotation curve

Before studying the non-circular motions, we must determine the main parameters of the circular rotation of our objects. Using the rotation curve derived from the same sample of objects allows us to avoid systematical effects due to the eventual inconsistency of the distance scales of two different samples.

We determine the parameters of the rotation curve based only on the Cepheids located within 3.5 kpc from the Sun ($r < 3.5$ kpc) and within 0.5 kpc ($|z| < 0.5$ kpc) from the Galactic plane. This subsample includes 257 Cepheids with available accurate line-of-sight velocities and 217 Cepheids with Hipparcos proper motions. The approach we use to solve the Bottlinger equations was described in detail in our earlier papers (Dambis et al. 1995; Mel'nik, Dambis & Rastorguev 1999; Mel'nik & Dambis 2009), so we do not repeat it here. We list the inferred parameters of the rotation curve and solar motion in Table 4, where Ω_0 is the angular rotation velocity $\Omega(R)$ at $R = R_0$; Ω_0' and Ω_0'' are its

Copyright line will be provided by the publisher

Table 4 Parameters of the rotation curve and the solar motion

Objects	Ω_0 km s^{-1} kpc^{-1}	Ω_0' km s^{-1} kpc^{-2}	Ω_0'' km s^{-1} kpc^{-3}	u_0 km s^{-1}	v_0 km s^{-1}	A km s^{-1} kpc^{-1}	σ_0 km s^{-1}	N
Cepheids all periods	28.8 ±0.8	-4.88 ±0.14	1.07 ±0.17	8.1 ±0.8	12.7 ±1.0	18.3 ±0.6	10.84	474
Cepheids $P < 8$d	30.0 ±1.0	-4.90 ±0.22	0.92 ±0.25	8.3 ±1.0	12.1 ±1.2	18.4 ±0.8	11.19	323
Cepheids $P > 8$d	27.0 ±1.1	-4.85 ±0.19	1.31 ±0.24	7.7 ±1.3	14.2 ±1.7	18.2 ±0.7	10.04	151
OB-associations	30.6 ±0.9	-4.73 ±0.18	1.43 ±0.21	7.7 ±1.0	11.6 ±1.3	17.7 ±0.7	7.16	132

first and second derivatives taken at $R = R_0$; u_0 and v_0 are the components of the solar motion with respect to the centroid of the sample in the direction toward the Galactic center and Galactic rotation, respectively; N is the number of conditional equations. Table 4 also includes the parameters derived for short- and long-period Cepheids separately and those for OB-associations.

Figure 8 (top panel) shows the rotation curve derived from an analysis of the line-of-sight velocities and proper motions of Cepheids of all periods. For comparison, we also show the rotation curve based on the data for OB-associations (Mel'nik & Dambis 2009). The parameters of the rotation curve derived for Cepheids and OB-associations agree within their errors, see Table 4. Our Cepheid sample yields $\Omega_0 = 28.8 \pm 0.8$ km s^{-1} kpc^{-1} which is also consistent with other studies of the Cepheid kinematics: $\Omega_0 = 27.2 \pm 0.9$ (Feast & Whitelock 1997) and $\Omega_0 = 27.5 \pm 0.5$ (Bobylev & Baikova 2012). However, there is a systematical difference between the value of Ω_0 obtained for Cepheids and that inferred for OB-associations and maser sources, $\Omega_0 = 31 \pm 1$ km s^{-1} (Reid et al. 2009a, Mel'nik & Dambis 2009; Bobylev & Baikova 2010). The linear rotation velocity at the solar Galactocentric distance estimated from the kinematics of Cepheids is systematically lower than the value derived from OB-associations. Moreover, the rotation curve of Cepheids seems to be slightly descending, whereas that of OB-associations is nearly flat within the 3 kpc neighborhood of the Sun. We are inclined to attribute these differences to the fact that the distances and proper motions available for Cepheids are less accurate than those of OB-associations. Averaging the distances and proper motions of stars within each OB-association may have given a considerable advantage. This problem requires further study.

The lower panel of Figure 8 shows the scatter of individual azimuthal velocities of Cepheids with respect to the rotation curve. The standard deviation of the projected velocities onto the Galactic plane from the rotation curve is $\sigma_0 = 10.8$ km s^{-1} for Cepheids of all periods.

We also calculated the parameters of the rotation curve for short- and long-period Cepheids (Table 4). It can be seen that parameters determined for Cepheids with $P < 8$ and $P > 8$ days are consistent within the errors except for Ω_0, which is conspicuously smaller for long-period Cepheids. Note that the standard deviation of the velocities from the rotation curve equals $\sigma_0 = 11.19$ and 10.04 km s^{-1} for short- and long-period Cepheids, respectively. The small difference between them suggests that both groups of Cepheids are suitable for study the Galactic structure.

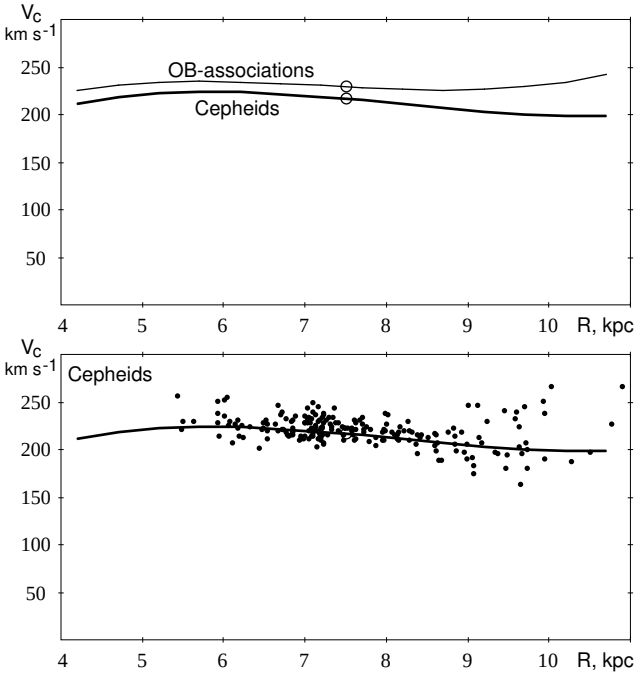

Fig. 8 Top panel: the Galactic rotation curve derived from an analysis of line-of-sight velocities and proper motions of Cepheids (thick line) and those of OB-associations (thin line). The position of the Sun is shown by a circle. Lower panel: the scatter of individual azimuthal velocities of Cepheids with respect to the rotation curve. It is built for Cepheids of all periods.

Copyright line will be provided by the publisher

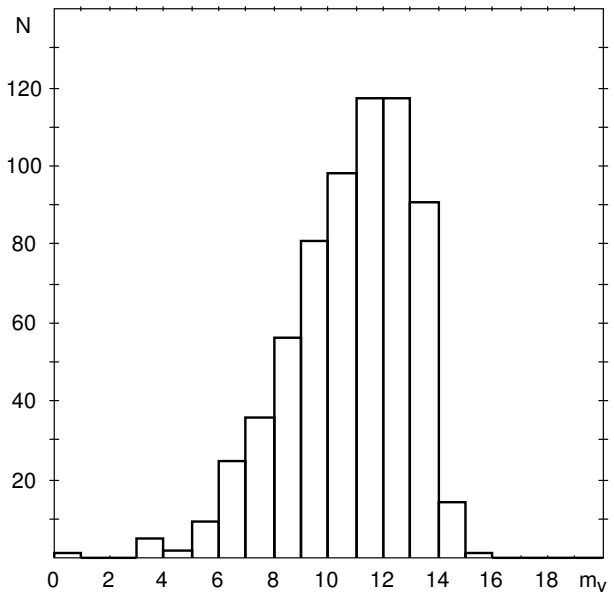

Fig. 9 The distribution apparent magnitudes m_v of classical Cepheids.

4.2 Residual velocities of Cepheids and model particles

Residual velocities characterize non-circular motions in the Galactic disk. We calculate the residual velocities for Cepheids as the differences between the observed heliocentric velocities and the computed velocities due to the circular rotation law and the adopted components of the solar motion defined by the parameters listed in Table 4 (first row). For model particles the residual velocities are determined with respect to the model rotation curve. We consider the residual velocities in the radial V_R and azimuthal V_T directions. Positive radial residual velocities V_R are directed away from the Galactic center while positive azimuthal residual velocities V_T are in the sense of Galactic rotation.

Figure 10 shows the distribution of model particles with negative and positive residual velocities V_R and V_T located within 3.5 kpc from the Sun. The left panel demonstrates the distribution of radial residual velocities V_R. Model particles in the outer ring R_1 (the one which is closer to the Galactic center) have positive velocities V_R (black circles), whereas those in the ring R_2 have negative velocities V_R (gray circles). Particles located at the Galactic periphery ($R > R_0 + 2$ kpc) have close to zero velocities V_R (black points). The right panel shows the distribution of azimuthal velocity V_T. Model particles in the ring R_1 lying left of the Sagittarius complex ($l \approx 15^\circ$, $r \approx 1.5$ kpc) have mostly negative V_T velocities while those situated right of it have mostly positive V_T velocities. It is not a chance coincidence because the position angle of the bar θ_b was chosen in such a way that model particles reproduce nearly zero velocities V_T of OB-associations in the Sagittarius complex (Mel'nik & Rautiainen 2009). In the ring R_2 we see the opposite velocity gradient: model particles located at the negative x-coordinates have mostly positive V_T velocities (black circles), whereas those situated at the positive x-coordinates have mainly negative V_T velocities (gray circles).

Let us consider the distribution of Cepheids and model particles with negative ($V_R < 0$) and positive ($V_R > 0$) radial residual velocities (Figure 11). The left panel shows the distribution of objects with negative radial velocities V_R which are supposed to belong to the outer ring R_2. Within $r < 3.0$ kpc from the Sun, the elliptic ring R_2 can be represented as a fragment of the spiral arm. Its pitch angle appears to be $i = 8.3 \pm 3.9^\circ$ and $i = 6.0 \pm 0.5^\circ$ for Cepheids and model particles, respectively. The positive value of the pitch angle i indicates that the spiral arm is leading and corresponds to the solar position near the descending segment of the outer ring R_2. Since the ring R_2 is aligned with the bar, the location of the Sun near the descending segment of the outer ring R_2 reflects the well-known fact that the bar's end closest to the Sun lies in quadrant I.

Figure 11 (right panel) shows Cepheids and model particles with positive radial residual velocities ($V_R > 0$). These objects are expected to concentrate to the ascending segment of the outer ring R_1. Unfortunately, we see no good agreement here. However, Cepheids do not occupy all the 3-kpc solar neighborhood, they as well as model particles with $V_R > 0$ are mostly located at negative y-coordinates.

Figure 12 shows the dependence of azimuthal velocity V_T on coordinate x for Cepheids and model particles with negative radial velocities ($V_R < 0$). The objects studied are located within 3 kpc of the Sun and are supposed to belong to the descending segment of the outer ring R_2. We consider only Cepheids with small errors ($\varepsilon_{vl} < 10$ km s^{-1}) of the tangential velocity in the Galactic plane V_l. The value of 10 km s^{-1} corresponds to the average deviation of the Cepheid velocity from rotation curve (σ_0 in Table 4). The error ε_{vl} is determined by the error of the proper motion in the Galactic plane μ_l and the distance r, $\varepsilon_{vl} = 4.74 r \varepsilon_{\mu_l}$, where proper motion is in mas yr^{-1} and the distance is in kpc. We use the linear law to describe the V_T-x relation: $V_T = ax + b$. The slope a for Cepheids and model particles appears to be $a = -2.0 \pm 0.8$ and $a = -3.3 \pm 0.1$, respectively. Both values of a are negative, and this trend for Cepheids has a significance level of $P > 2\sigma$.

Generally, the kinematical features obtained for Cepheids with negative radial velocities V_R are consistent with the solar location near the descending segment of the outer ring R_2.

5 Discussion and conclusions

We use the data from the catalog by Berdnikov et al. (2000) to study the distribution and kinematics of classical Cepheids in terms of the model of the Galactic ring $R_1 R_2'$ (Mel'nik & Rautiainen 2009). The best agreement between the distribution of Cepheids located within $r_{max} =$ 2.5, 3.0, and 3.5 kpc from the Sun and the model of the outer

Copyright line will be provided by the publisher

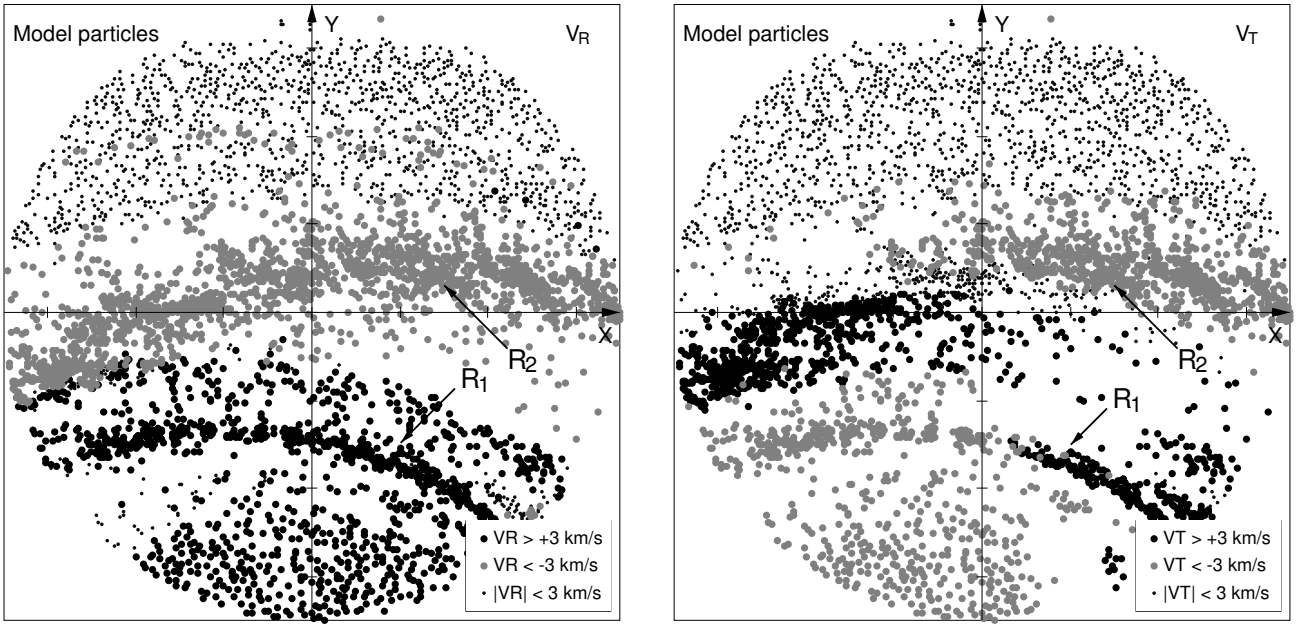

Fig. 10 Distribution of negative and positive residual velocities V_R (left panel) and V_T (right panel) calculated for model particles located in the solar neighborhood of 3.5 kpc. The radial velocities V_R are subdivided into three groups: negative ($V_R < -3$ km s^{-1}), positive ($V_R > +3$ km s^{-1}) and close to zero ($|V_R| < 3$ km s^{-1}). The same was done for the azimuthal velocities V_T. The solar position angle θ_b for model particles is chosen to be $\theta_b = 45^\circ$. The arrows show the locations of the fragments of the outer rings R_1 and R_2: the ring R_1 is closer to the center than the ring R_2. The X-axis is directed in the sense of the Galactic rotation, the Y-axis is directed away from the Galactic center. The Sun is in the origin. One tick interval along the X- and Y-axis corresponds to 1 kpc.

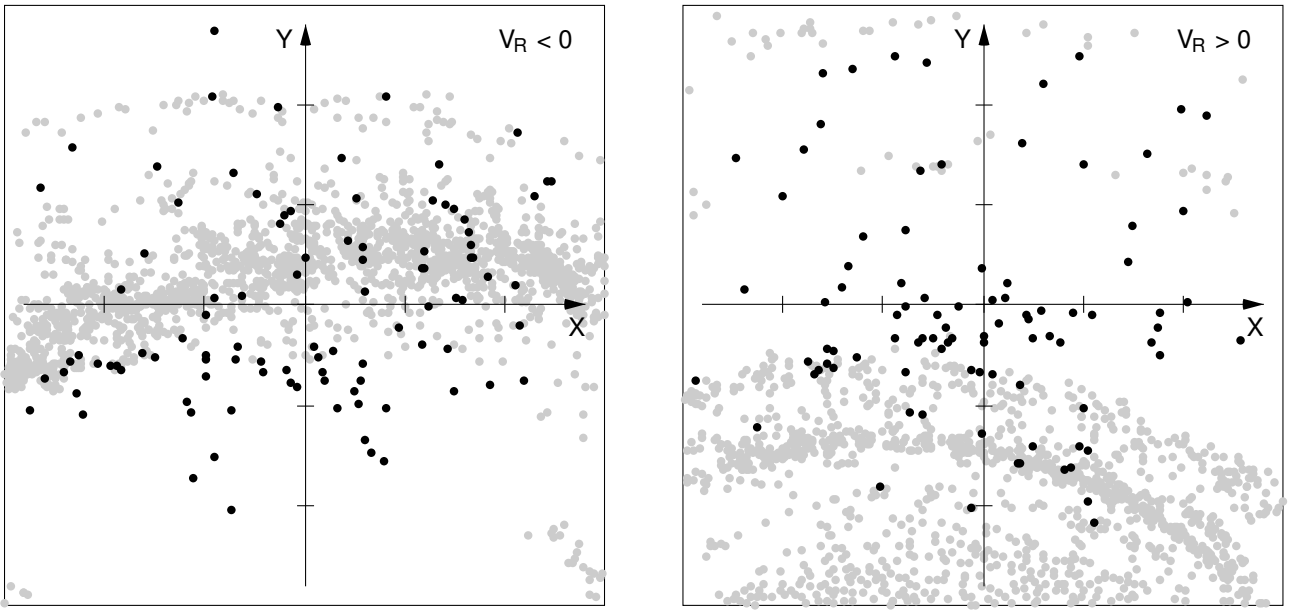

Fig. 11 Distribution of Cepheids (black circles) and model particles (gray circles) with negative ($V_R < 0$) and positive ($V_R > 0$) radial residual velocities in the Galactic plane. Left: objects with $V_R < 0$ are supposed to belong to the descending segment of the outer ring R_2. Right: objects with the positive radial residual velocities ($V_R > 0$) are mostly located in quadrants I and IV. The X-axis is directed in the sense of the Galactic rotation, the Y-axis is directed away from the Galactic center. The Sun is at the origin. One tick interval along the X- and Y-axis corresponds to 1 kpc.

Copyright line will be provided by the publisher

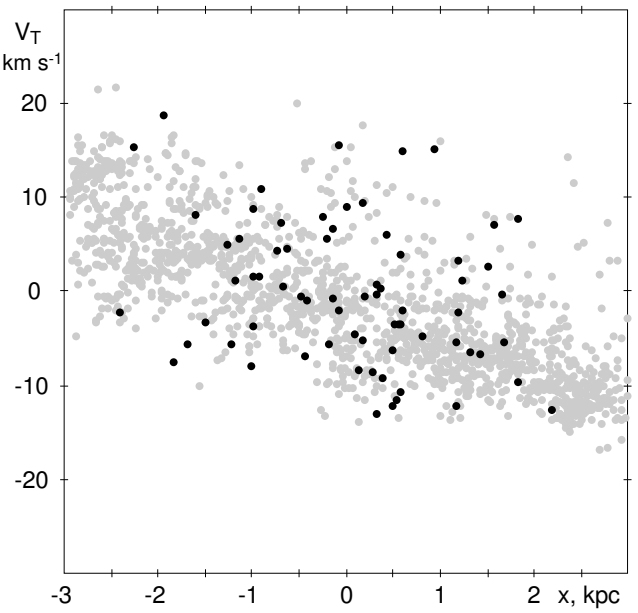

Fig. 12 Dependence of azimuthal velocity V_T on coordinate x for the Cepheids (black circles) and model particles (gray circles) with negative radial residual velocities ($V_R < 0$). These objects are supposed to belong to the descending segment of the outer ring R_2. Both Cepheids and model particles demonstrate a decrease in V_T with increasing x.

ring R_1R_2' is obtained if the position angle of the Sun with respect to the bar major axis is $\theta_b = 50 \pm 5°$, $37 \pm 5°$, and $25 \pm 5°$, respectively. Averaging these values gives the final estimate of $\theta_b = 37 \pm 13°$. It is "the fork-like" structure in the distribution of Cepheids that determines the angle θ_b being close to 45°: at longitudes $l > 180°$ two outer rings fuse together to form one spiral fragment – the Carina arm, whereas at longitudes $l < 180°$ two outer rings run separately producing the Sagittarius and Perseus arm-fragments.

To study the surface density n and extinction A_V of Cepheids in different directions, we subdivide the sample into four sectors and calculate the average values of n and A_V at different heliocentric distances r. The surface density n of Cepheids appears to drop sharply in the direction of the Galactic center ($|l| < 45°$). Furthermore, extinction A_V grows most rapidly just in this direction. These features can be due to the presence of the ring R_1 located in the direction of the Galactic center at 1–2 kpc from the Sun.

Our analysis of variations in the surface density of Cepheids along distance gives us the estimate of the completeness radius of the sample which appears to lie in the 2-4 kpc interval for the different sectors. A similar result was obtained from an analysis of distance moduli and visual magnitudes. We adopt 3 ± 1 kpc as the average value. Probably, within 3 kpc from the Sun, the apparent distribution of known Cepheids reflects their physical distribution rather than instrumental-related difficulties in their discovery and study.

The parameters of the rotation curve derived from the samples of Cepheids and OB-associations (Mel'nik & Dambis 2009) are consistent within the errors (Table 4).

We study the distribution of Cepheids and model particles with negative radial residual velocities ($V_R < 0$), which inside 3 kpc of the Sun must belong to the outer ring R_2. The selected Cepheids and model particles demonstrate similar distribution in the Galactic plane: both samples concentrate to the fragment of the leading spiral arm with the pitch angle of $i = 8.3 \pm 3.9°$ and $i = 6.0 \pm 0.5°$, respectively. A similar leading fragment was found in the distribution of OB-associations with negative radial residual velocities ($V_R < 0$) (Mel'nik 2005). The appearance of the leading fragment suggests that the Sun is located near the descending segment of the ring R_2. Moreover, selected Cepheids and model particles exhibit similar variations of azimuthal velocity V_T in the direction of Galactic rotation (the x coordinate).

All this morphological and kinematical evidence suggests the existence of a ring R_1R_2' in the Galaxy. N-body simulations show that the descending segments of the outer rings R_2 often include clumps and spurs (Rautiainen & Salo 2000). Probably, the Galactic outer ring R_2 is not homogeneous in the solar neighborhood. The local Cygnus arm ($l = 70$–$80°$, $r = 1$–2 kpc) and the observed fragment of the Perseus arm ($l = 100$–$140°$, $r = 1.5$–3.0 kpc) can be associated with some of these model spurs. Such spurs usually have a larger pitch angle than large-scale patterns like segments of elliptical rings or global spiral arms. The nature of the fragmentation is not clear, it can be of purely hydrodynamical origin (Dobbs & Bonnell 2006) or be associated with slow modes forming in the stellar population of the disk (Rautiainen & Salo 1999, 2000).

Acknowledgements. We thank H. Salo for sharing his N-body code. This work was supported in part by the Russian Foundation for Basic Research (project nos. 12-02-00827, 13-02-00203, 14-02-00472). Calculations of the light-curve parameters and gamma-velocities of Cepheids were supported by Russian Scientific Foundation grant no. 14-22-00041.

Funding for SDSS-III has been provided by the Alfred P. Sloan Foundation, the Participating Institutions, the National Science Foundation, and the U.S. Department of Energy Office of Science. The SDSS-III web site is http://www.sdss3.org/.

SDSS-III is managed by the Astrophysical Research Consortium for the Participating Institutions of the SDSS-III Collaboration including the University of Arizona, the Brazilian Participation Group, Brookhaven National Laboratory, Carnegie Mellon University, University of Florida, the French Participation Group, the German Participation Group, Harvard University, the Instituto de Astrofisica de Canarias, the Michigan State/Notre Dame/JINA Participation Group, Johns Hopkins University, Lawrence Berkeley National Laboratory, Max Planck Institute for Astrophysics, Max Planck Institute for Extraterrestrial Physics, New Mexico State University, New York University, Ohio State University, Pennsylvania State University, University of Portsmouth, Princeton University, the Spanish Participation Group, University of Tokyo, University of Utah, Vanderbilt University, University of Virginia, University of Washington, and Yale University.

Copyright line will be provided by the publisher

References

Athanassoula, E.: 1984, Phys. Rep. 114, 321
Athanassoula, E., Romero-Gómez, M., Bosma, A., Masdemont, J.J.: 2010, MNRAS 407, 1433
Baba, J., Asaki, Y., Makino, J., Miyoshi, M., Saitoh, T., Wada, K.: 2009, ApJ 706, 471
Barbier-Brossat, M., Petit, M., Figon, P.: 1994, A&AS 108, 603
Benjamin, R.A., Churchwell, E., Babler, B.L., et al.: 2005, ApJ 630, L149
Berdnikov, L.N., Dambis, A.K., Vozyakova, O.V.: 2000, A&AS 143, 211
Berdnikov, L.N., Dambis, A.K., Vozyakova, O.V.: 2014, in preparation
Berdnikov, L.N., Kniazev, A.Yu., Kravtsov, V.V., Pastukhova, E.N., Turner, D.G.: 2009a, Astron. Lett. 35, 39
Berdnikov, L.N., Kniazev, A.Yu., Kravtsov, V.V., Pastukhova, E.N., Turner, D.G.: 2009b, Astron. Lett. 35, 311
Berdnikov, L.N., Kniazev, A.Yu., Sefako, R., Kravtsov, V.V., Pastukhova, E.N., Zhuiko, S.V.: 2011, Astron. Rep. 55, 816
Berdnikov, L.N., Kniazev, A.Yu., Sefako, R., Kravtsov, V.V., Zhuiko, S.V.: 2014, Astron. Lett. 40, 125
Berdnikov, L.N., Vozyakova, O.V., Dambis, A.K.: 1996a, Astron. Lett. 22, 334
Berdnikov, L.N., Vozyakova, O.V., Dambis, A.K.: 1996b, Astron. Lett. 22, 839
Binney, J., Gerhard, O., Stark, A.A., Bally, J., Uchida, K.I.: 1991, MNRAS 252, 210
Bissantz, N., Englmaier, P., Gerhard, O.: 2003, MNRAS 340, 949
Blanton, M.R., Kazin, E., Muna, D., Weaver, B.A., Price-Whelan, A.: 2011, ApJ 142, 31
Blitz, L., Spergel, D.N.: 1991, ApJ 379, 631
Bobylev, V.V., Baikova, A.T.: 2010, MNRAS 408, 1788
Bobylev, V.V., Baikova, A.T.: 2012, Astron. Lett. 38, 638
Bono, G., Marconi, M., Cassisi, S., Caputo, F., Gieren, W., Pietrzynski, G.: 2005, ApJ 621, 966
Burton, W.B., Bania, T.M.: 1974, A&A 33, 425
Buta, R.: 1995, ApJS 96, 39
Buta, R., Combes, F.: 1996, Fund. Cosmic Physics 17, 95
Buta. R., Corwin H.G., Odewahn S.C.: 2007, The de Vaucouleurs Atlas of Galaxies, Cambridge Univ. Press.
Buta, R., Crocker, D.A.: 1991, AJ 102, 1715
Byrd, G., Rautiainen, P., Salo, H., Buta, R., Crocker, D.A.: 1994, AJ 108, 476
Cabrera-Lavers, A., Hammersley, P.L., González-Fernández, C., López-Corredoira, M., Garzón, F., Mahoney, T.J.: 2007, A&A 465, 825
Churchwell, E., Babler, B.L., Meade, M.R., et al.: 2009, PASP 121, 213
Comerón, S., Salo, H., Laurikainen, E., et al.: 2014, A&A 562, 121
Contopoulos, G., Grosbol, P.: 1989, A&AR 1, 261
Contopoulos, G., Papayannopoulos, Th.: 1980, A&A 92, 33
Contopoulos, G, Patsis, P.A.: 2006, MNRAS 369, 1039
Dambis, A.K., Berdnikov, L.N., Kniazev, A.Y., Kravtsov, V.V., Rastorguev, A.S., Sefako, R., Vozyakova, O.V.: 2013, MNRAS 435, 3206
Dambis, A.K., Mel'nik, A.M., Rastorguev, A.S.: 1995, Astron. Lett. 21, 291
Dame, T.M., Hartmann, D., Thaddeus, P.: 2001, ApJ 547, 792
Dean, J.F., Warren, P.R., Cousins, A.W.J.: 1978, MNRAS 183, 569
Debattista, V.P., Sellwood, J.A.: 2000, ApJ 543, 704
Dehnen, W.: 2000, AJ 119, 800
Dobbs, C.L., Bonnell, I. A.: 2006, MNRAS 367, 873
Efremov, Yu.N.: 2003, Astron. Rep. 47, 1000
Efremov, Y.N., Sitnik, T.G.: 1988, Soviet Astron. Lett. 14, 347
Englmaier, P., Gerhard, O.: 1999, MNRAS 304, 512
ESA 1997, The Hipparcos and Tycho Catalogs: ESA SP-1200, Noordwijk
Feast, M.W., Laney, C.D., Kinman, T.D., van Leeuwen, F., Whitelock, P.A.: 2008, MNRAS 386, 2115
Feast, M.W., Whitelock, P.A.: 1997, MNRAS 291, 683
Fernie, J.D., Evans, N.R., Beattie, B., Seager, S.: 1995, IBVS 4148, 1
Fux, R.: 2001, A&A 373, 511
Georgelin, Y.M., Georgelin, Y.P.: 1976, A&A 49, 57
Glushkova, E.V., Dambis, A.K., Mel'nik, A.M., Rastorguev, A.S.: 1998, A&A 329, 514
González-Fernández, C., López-Corredoira, M., Amôres, E. B., Minniti, D., Lucas, P., Toledo, I.: 2012, A&A 546, 107
Gorynya, N.A., Irsmambetova, T. R., Rastorguev, A.S., Samus, N.N.: 1992, Sov. Astron. Lett. 18, 316
Gorynya N.A., Rastorguev, A.S.: 2014, in prepapration
Gorynya, N.A., Samus, N.N., Sachkov, M.E., Rastorguev, A.S., Glushkova, E.V., Antipin, S.V.: 1998, Astron. Lett. 24, 815
Gorynya, N.A., Samus, N.N., Sachkov, M.E., Rastorguev, A.S., Glushkova, E.V., Antipin, S.V.: 2002, VizieR On-line Data Catalog: III/229
Groenewegen, M.A.T., Udalski, A., Bono, G.: 2008, A&A 481, 441
Harsoula, M., Kalapotharakos, C.: 2009, MNRAS 394, 1605
Hertzsprung, E.: 1926, Bull. Astron. Netherlands 3, 115
Kalnajs, A.J.: 1991, Pattern Speeds of Density Waves, in Dynamics of Disc Galaxies, ed. B. Sundelius (Göteborgs Univ., Göthenburg), p. 323
Lin, C.C., Yuan, C., Shu, F.H.: 1969, ApJ 155, 721
Masset, F., Tagger, M.: 1997, A&A 322, 442
Malaroda, S., Levato, H., Galliani, S.: 2006, VizieR On-line Data Catalog: III/249
Mel'nik, A.M.: 2003, Astron. Lett. 29, 304
Mel'nik, A.M.: 2005, Astron. Lett. 31, 80
Mel'nik, A.M., Dambis, A.K.: 2009, MNRAS 400, 518
Mel'nik, A.M., Dambis, A.K., Rastorguev, A.S.: 1999, Astron. Lett. 25, 518
Mel'nik, A.M., Dambis, A.K., Rastorguev, A.S.: 2001, Astron. Lett. 27, 521
Mel'nik, A.M., Rautiainen, P.: 2009, Astron. Lett. 35, 609
Mel'nik, A.M., Rautiainen, P.: 2011, MNRAS 418, 2508
Mel'nik, A.M., Rautiainen, P.: 2013, AN 334, 777
Metzger, M.R., Caldwell, J.A.R., McCarthy J.K., Schechter, P.J.: 1991, ApJS 76, 803
Metzger, M.R., Caldwell, J.A.R., Schechter, P.J.: 1992, AJ 103, 529
Metzger, M.R., Caldwell, J.A.R., Schechter, P.J.: 1998, AJ 115, 635
Nikiforov, I.I.: 2004, The Distance to the Center of the Galaxy: the Current State-of-the-Art in Measuring R_0, in Order and Chaos in Stellar and Planetary Systems, ed. G.G. Byrd, K.V. Kholshevnikov, A.A. Mylläri, I.I. Nikiforov, & V.V. Orlov, ASPC 316 (ASP, San Francisco), 199
Pojmanski, G.:2002, AcA 52, 397
Pont, F., Mayor, M., Burki, G.: 1994, A&A 285, 415
Pont, F., Queloz, D., Bratschi, P., Mayor, M.: 1997, A&A 318, 416
Press, W.H., Flannery, B.P., Teukolsky, S.A., Wetterling, W.T., Kriz, S.: 1987, Numerical Recipes, The Art of Scientific Computing, Cambridge Univ. Press, Cambridge

Copyright line will be provided by the publisher

Rastorguev, A.S., Pavlovskaya, E.D., Durlevich, O.V., Filippova, A.A.: 1994, Astron. Lett. 20, 591
Rautiainen, P., Mel'nik, A.M.: 2010, A&A 519, 70
Rautiainen, P., Salo, H.: 1999, A&A 348, 737
Rautiainen, P., Salo, H.: 2000, A&A 362, 465
Reid, M.J., Menten, K.M., Brunthaler, A., Zheng, X.W., Moscadelli, L., Xu, Y.: 2009a, ApJ 693, 397
Reid, M.J., Menten, K.M., Zheng, X.W., Brunthaler, A., Xu, Y.: 2009b, ApJ 705, 1548
Romero-Gómez, M., Athanassoula, E., Masdemont, J.J., García-Gómez, C.: 2007, A&A 472, 63
Russeil, D.: 2003, A&A 397, 133
Saito, R.K., Hempel, M., Minniti, D., at al.: 2012, A&A 537, 107
Salo, H.: 1991, A&A 243, 118
Salo, H., Laurikainen, E.: 2000, MNRAS 319, 377
Samus, N.N., Durlevich, O.V., Goranskij, V.P., Kazarovets, E.V., Kireeva, N.N., Pastukhova, E.N., Zharova, A.V.: 2007, General Catalogue of Variable Stars (Samus+ 2007-2013), VizieR On-line Data Catalog: B/gcvs
Sandage, A., Tammann, G.A.: 2006, ARA&A 44, 93
Schwarz, M.P.: 1981, ApJ 247, 77
Sellwood, J.A.: 2000, Ap&SS 272, 31
Sellwood, J.A.: 2010, MNRAS 409, 145
Sellwood, J.A., Carlberg, R.G.: 1984, ApJ 282, 61
Sellwood, J.A., Sparke, L.S.: 1988, MNRAS 231, 25
Sheth, K., Regan, M., Hinz, J.L., et al.: 2010, PASP 122, 1397
Sitnik, T.G.: 2003, Astron. Lett. 29, 311
Szabados, L.: 2003, Cepheids: observational properties, binarity and GAIA, in GAIA Spectroscopy: Science and Technology, ed. U. Munari, ASPC 298 (ASP, San Francisco), 237
Toomre, A.: 1977, ARA&A 15, 437
Treuthardt, P., Salo, H., Rautiainen, P., Buta, R.: 2008, AJ 136, 300
Vallée, J.P.: 2008, AJ 135, 1301
Vallée, J.P.: 2013, Intern. J. A&A 3, 20
van Leeuwen, F.: 2007, A&A 474, 653
Voglis, N., Harsoula, M., Contopoulos, G.: 2007, MNRAS 381, 757
Weiner, B.J., Sellwood, J.A.: 1999, ApJ 524, 112
York, D.G., et al.: 2000, ApJ 120, 1579
Zabolotskikh, M.V., Rastorguev, A.S., Dambis A.K.: 2002, Astron. Lett. 28, 454

Copyright line will be provided by the publisher